

Mesoporous activated carbon from *Pentace* species sawdust via microwave-induced KOH activation: optimization and methylene blue adsorption

Azduwin Khasri^{1,3} · Olugbenga Solomon Bello² ·
Mohd Azmier Ahmad³ 

Received: 18 January 2018 / Accepted: 24 April 2018 / Published online: 4 May 2018
© Springer Science+Business Media B.V., part of Springer Nature 2018

Abstract This work studied the optimization of preparation conditions of *Pentace* species sawdust activated carbon (PSAC) via microwave-induced KOH activation for the adsorption of methylene blue (MB) dye from aqueous solutions. The produced activated carbon was characterised through Brunauer–Emmett–Teller (BET) surface area and pore structural analysis, proximate and ultimate, scanning electron microscopy, and Fourier transform infrared spectroscopy. Response surface methodology technique was used to optimize the radiation power, radiation time and impregnation ratio for MB removal and PSAC yield through central composite design. The optimum preparation conditions for PSAC were obtained at a radiation power of 418 W, radiation time of 6.4 min, and an impregnation ratio of 0.5, which resulted in 27% PSAC yield and 93.74% MB removal. A mesoporous structure of PSAC was formed, with a BET surface area, total pore volume and average pore diameter of 914.15 m²/g, 0.52 cm³/g, and 3.19 nm, respectively. The experimental kinetic data were well described by a pseudo-second-order model and intraparticle diffusion. Adsorption data fitted the Redlich–Peterson equation better than the

✉ Mohd Azmier Ahmad
chazmier@usm.my

Azduwin Khasri
azduwin@unimap.edu.my

Olugbenga Solomon Bello
osbello@lautech.edu.ng

¹ Department of Chemical Engineering Technology, Faculty of Engineering Technology, Universiti Malaysia Perlis, Kampus Unicity Sungai Chuchuh, 02100 Padang Besar, Perlis, Malaysia

² Department of Pure and Applied Chemistry, Ladoke Akintola University of Technology, P.M.B 4000, Ogbomoso, Oyo State, Nigeria

³ School of Chemical Engineering, Engineering Campus, Universiti Sains Malaysia, 14300 Nibong Tebal, Pulau Pinang, Malaysia

Langmuir, Freundlich, Temkin, Dubinin–Radushkevich and Sips equations. However, the exponential value of Redlich–Peterson approached unity, hence, resulting in the original Langmuir equation, with adsorption capacity of 357.14 mg/g. The adsorption performance was effectively preserved even after four consecutive cycles, demonstrating good regeneration ability.

Keywords Activated carbon · *Pentace* species sawdust · Methylene blue · Optimization · Adsorption isotherm · Kinetics

Introduction

Dye effluents are among the main contributors to water pollution [1]. More than 10,000 tonnes of dyes are produced every year. During dye production, large quantities of dye effluents are generated and serious water pollution is caused [2]. Several methods have recently been implemented for the removal of textile dyes from wastewater, such as chemical oxidation, anaerobic treatment, adsorption, biosorption, coagulation, membrane filtration and photocatalysis [3]. The effectiveness of adsorption processes as good physical separation methods to remove dyes from aqueous solution can no longer be denied, due to simple operation requirements, non-sensitivity to toxic substances, and flexibility in activated carbon (AC) selection from various sources [4]. Carbonisation and activation are two processes that are usually performed in the preparation of AC. Several complex reactions occur which release volatile compounds and produce fixed carbon mass during the carbonisation process [5]. On the other hand, the activation process can be performed by either chemical and/or physical methods, or both simultaneously.

In chemical activation, the raw material is physically mixed or impregnated with activating agents such as $ZnCl_2$, NaOH, H_3PO_4 , KOH, and K_2CO_3 to create the pore structure [6]. Among the chemical activation agents, KOH is usually preferred as it is more eco-friendly than other activators. In addition, the formation of K_2CO_3 that occurs after the interaction between KOH and char can prevent excessive burning of the sample, resulting in higher yield and producing good porosity [7]. The process of chemical activation from different types of precursor using KOH as a chemical agent has recently been reported by several researchers [8–11].

In a preparation of AC, conventional heating methods using tubular furnaces are normally used, in which energy is generated by convective or conductive heating systems [12]. Nevertheless, in some cases this thermal heating may take a longer time to achieve the preferred phase of activation [13]. Another disadvantage of conventional heating is its lack of uniformity when heating samples of dissimilar shapes and sizes, whereby it produces a thermal gradient from the outer hot surface of the particle to its inner parts, and blocks the effective removal of gaseous products to the atmosphere which, in turn, can damage the quality of the prepared AC [14]. Lately, heating systems employing microwave irradiation have been widely used for the preparation of AC. The microwave energy is transferred to the interior part of the samples by dipole rotation and ionic conduction, rather than by

conduction and convection [15]. Consequently, microwave heating results in a significantly reduced treatment time. The removal of dyes from wastewater using activated-carbon adsorbents prepared by microwave-assisted activation from various source such as date stones [16], coconut shells [17], pomegranate peel [9], oil palm shells [18], peanut shells [19], coffee shells [20], palm kernel shells [21], *Jatropha* [22] and rice husks [23] have been studied by many investigators.

Pentace species, with various common names such as Melunak (Malaysia), Burma mahogany (Myanmar), or Sisiat pluak (Thailand) belong to a genus of 34 tree species such as *Pentace burmanica*, *Pentace triptera* and many more. The wood processing residues are comprised of sawdust, slabs, off-cuts, shavings and chips, which make up about 20% of the total input mass [24]. In some wood-processing factories, these residues remain unused and are disposed of either by burning or disposal in landfills. To address this issue, in this study, the use of microwave irradiation for the preparation of AC from *Pentace* species sawdust (PS) via KOH activation was explored. Over the years, several papers have reported the successful use of several types of wood sawdust precursors for the potential preparation of AC using different activation methods [25–30]. Therefore, the present work focuses on optimizing the conditions for the microwave preparation of PSAC through varying the radiation power, radiation time and impregnation ratio, based on RSM, with the purpose of removing MB dye from aqueous solutions. The isotherms, kinetics and desorption study of PSAC were also studied.

Materials and methods

Materials

Locally obtained PS was thoroughly washed to remove dirt and other unwanted materials, dried and sieved to a particle size of 0.5–1 mm. Potassium hydroxide, KOH (85%), purchased from Riedel–de–Haen, Germany, was used as the activating agent. MB supplied by Sigma-Aldrich (M) Sdn Bhd, Malaysia, was used as the adsorbate. N₂ and CO₂ gases were supplied by MOX Gases, Berhad, Malaysia and were of 99.99 and 98.00% purity, respectively.

Synthesis of activated carbon

In the carbonisation process, 30 g of dried sawdust was loaded into a vertical tubular reactor made from stainless steel which was placed in a furnace. The sample was then heated to 700 °C for 2 h under a nitrogen flow (flow rate = 150 cm³/min; heating rate = 10 °C/min). The char produced was impregnated with KOH at various impregnation ratios (IRs) (0.5–2.0 g/g) and dehydrated at 110 °C for 24 h in an oven.

The microwave activation step was performed using a conventional 2.45 GHz microwave oven that was modified to accommodate the reactor and the inlet and outlet of gases. Microwave-induced activation of the impregnated char with KOH was conducted at different powers: 264, 440 and 616 W, and various radiation

times: 4, 6, and 8 min, with continuous flow of CO₂ gas at 300 cm³/min. The sample was rinsed repeatedly with deionised water and 0.1 M hydrochloric acid to reach pH 7. The AC obtained was dried at 110 °C for 24 h.

Optimization using RSM

Standard RSM with CCD was used to optimize the effective parameters with the least possible number of experiments, and in addition to analyse the relation between them [31]. In this work, the variables considered were radiation power (x_1), radiation time (x_2), and impregnation ratio (x_3). The ranges and the levels of these variables are listed in Table 1.

A total of 20 experiments were performed for the three factors ($= 2^3 + 2(3) + 6$) which consisted of 14 experiments plus six replicate parameters to evaluate the pure error. Because only three stages were attributed to each factor, the corresponding model is a quadratic model, expressed by Eq. (1):

$$Y = b_0 + \sum_{i=1}^n b_i x_i + \sum_{i=1}^n b_{ii} x_i^2 + \sum_{i=1}^{n-1} \sum_{j=i+1}^n b_{ij} x_i x_j + e_i, \quad (1)$$

where Y is the predicted response, b_0 is the constant coefficient, b_i the linear coefficient, b_{ij} the interaction coefficient, b_{ii} the quadratic coefficient, x_i and x_j the coded values of the AC preparation variables, and e_i is the error. Design Expert Software (version 6.0.7) was used for further regression analyses, analyses of variance (ANOVA), and response surfaces.

Characterisation of PSAC

The total pore volumes and average pore diameters of the samples were determined using a Micromeritics ASAP 2020 volumetric adsorption analyser. The BET surface area was determined from the adsorption isotherm using the BET equation. The surface morphologies of the samples were examined using SEM (LEO SUPRA 55VP, Germany). Proximate analyses were carried out using a simultaneous thermal analyser (Perkin Elmer STA 6000, USA), and the elemental compositions of the samples were determined using an elemental analyser (Perkin Elmer Series II 2400, USA). The functional groups on the surface of the PS and PSAC were characterised by FTIR (Shimadzu Prestige 21, Japan).

Table 1 Experimental factors

Variable (factor)	Code	Units	Coded values		
			-1	0	+1
Radiation power	x_1	W	264	440	616
Radiation time	x_2	Min	4	6	8
Impregnation Ratio (IR)	x_3	–	0.50	1.25	2.00

Batch adsorption studies

Adsorption experiments were carried out by adding 0.20 g of PSAC into 250 mL Erlenmeyer flasks containing 200 mL of MB dye solutions with different initial concentration (25, 50, 100, 200, 250 and 300 mg/L) and agitating at 120 rpm at 30 °C until equilibrium was reached. A UV-vis spectrophotometer (Agilent Cary 60) was used to determine the concentration of each MB dye solution at wavelength maximum of 668 nm. The interactions between the adsorbate and the adsorbent were analysed using six isotherm equations, namely Langmuir [32], Freundlich [33], Temkin [34], Dubinin–Radushkevich [35], Redlich–Peterson [36] and Sips [37]. Isotherm parameters for MB dye adsorption on PSAC are listed in Table 2.

In order to find the best fit among the adsorption isotherm models, the correlation coefficients, R^2 and the Chi square (χ^2) tests were carried out. The correlation coefficient R^2 value, which was close to unity, showed that the model fitted the data well, while the lower value of χ^2 indicated that difference was not significant [34]. The Chi square statistical (χ^2) equation was given by:

$$\chi^2 = \sum \left(\frac{(q_{e,exp} - q_{e,cal})^2}{q_{e,cal}} \right) \tag{2}$$

Table 2 Isotherm and kinetic models

Model	Type	Expression
Isotherm	Langmuir	$q_e = \frac{q_m K_L C_e}{1 + K_L C_e}$ $R_L = \frac{1}{(1 + K_L C_e)}$
	Freundlich	$q_e = K_F C_e^{\frac{1}{n_F}}$
	Temkin	$q_e = B \ln(A) + B \ln(C_e)$
	Dubinin–Radushkevich	$q_e = q_D \exp(-B_{DR} \varepsilon^2)$ $E = \left[\frac{1}{\sqrt{2B_{DR}}} \right]$
	Redlich–Peterson	$q_e = \frac{K_R C_e}{1 + \alpha_R C_e^g}$
	Sips	$q_e = q_S \left[\frac{K_S C_e^{n_S}}{1 + K_S C_e^{n_S}} \right]$
Kinetic	Pseudo-first-order	$\ln(q_e - q_t) = \ln q_e - k_1 t$
	Pseudo-second-order	$\frac{t}{q_t} = \frac{1}{k_2 q_e^2} + \frac{1}{q_e} t$
	Elovich	$q_t = \frac{1}{\beta} \ln(\alpha \beta) + \frac{1}{\beta} \ln t$
	Intraparticle diffusion	$q_t = k_{it} t^{1/2}$

q_m = maximum adsorption capacity; K_L = Langmuir constant; R_L = separation factor; K_F and n_F = Freundlich constants; $B = RT/b$ is related to the heat of adsorption; A = dimensionless Temkin isotherm constant; B_{DR} = the mean free energy of adsorption, q_D = theoretical saturation capacity, ε = Polanyi potential, equal to $RT \ln(1 + (1/C_e))$; E = sorption energy; K_R and α_R = Redlich–Peterson isotherm constants; g = isotherm exponent; q_S = Sips capacity; K_S , n_S , Sips constants; k_1 and k_2 = rate constants for pseudo-first- and pseudo-second-order adsorptions; α = sorption constant of the adsorbate; β = desorption constant; k_{it} = intraparticle diffusion rate constant

Batch kinetic studies

Four widely used kinetic models were employed, such as pseudo-first-order (PFO) [38], pseudo-second-order (PSO) [39], Elovich [40] and intraparticle diffusion [34] kinetic models. Table 2 lists the equations and parameters of the kinetic models used in this study. The suitability of each kinetic model for the description of the adsorption process was further determined by calculating the normalised standard deviation, Δq (%), as given by Eq. (3):

$$\Delta q = 100 \sqrt{\frac{\sum [(q_{\text{exp}} - q_{\text{cal}})/q_{\text{exp}}]^2}{n - 1}}. \quad (3)$$

Desorption studies

The reusability of the PSAC was evaluated using the ethanol desorption method [41]. Once the adsorption equilibrium is reached, the amount of adsorption is determined from the difference in initial concentration and concentration at equilibrium. The spent AC was separated from the solution and rinsed with distilled water to eliminate any unadsorbed MB dye. For the desorption process, the samples were dried at 110 °C in an oven for 12 h before being added to an Erlenmeyer flask containing 200 mL of ethanol (95 vol%). The same adsorption process was conducted on the sample, and then these two processes were repeated four times. The regeneration efficiency was measured using Eq. (4):

$$\text{Desorption (\%)} = \frac{C_{\text{de}}}{C_{\text{ad}}} \times 100, \quad (4)$$

where C_{de} (mg/L) is the equilibrium concentrations of MB dye in the desorption process and C_{ad} (mg/L) denotes the difference between the initial and equilibrium concentrations of MB dye in the adsorption process.

Results and discussion

RSM and model fit

The experimental values for MB removal and PSAC yield are listed in Table 3. For both responses, the quadratic model was selected and the final empirical formulas for MB removal (Y_1) and PSAC yield (Y_2), in terms of the coded factors, after excluding the insignificant terms, are given by Eqs. (5) and (6), respectively.

$$Y_1 = 94.66 - 17.2x_1 - 0.91x_3 - 4.15x_1x_2 - 5.82x_1x_3 - 4.07x_2x_3 - 17.25x_1^2 - 3.35x_2^2 - 3.01x_3^2 \quad (5)$$

Table 3 Experimental factor condition and responses (condition: initial concentration 100 mg/L)

Run no.	Type	Factors			Responses	
		x_1 : Radiation power (w)	x_2 : Radiation time (Min)	x_3 : IR	Y_1 : MB Removal (%)	Y_2 : PSAC yield (%)
19	Fact	264	4	0.50	75.44	36.80
8	Fact	616	4	0.50	60.33	24.50
20	Fact	264	8	0.50	91.67	33.10
15	Fact	616	8	0.50	60.56	22.01
17	Fact	264	4	2.00	93.00	36.90
10	Fact	616	4	2.00	55.22	24.50
12	Fact	264	8	2.00	93.53	33.40
6	Fact	616	8	2.00	38.56	21.87
5	Axial	264	6	1.25	94.00	34.90
14	Axial	616	6	1.25	61.00	23.60
3	Axial	440	4	1.25	91.70	29.00
13	Axial	440	8	1.25	91.10	25.00
2	Axial	440	6	0.50	92.43	24.00
4	Axial	440	6	2.00	91.05	25.00
16	Centre	440	6	1.25	94.00	26.10
11	Centre	440	6	1.25	94.00	26.30
1	Centre	440	6	1.25	94.89	25.70
18	Centre	440	6	1.25	94.90	25.90
7	Centre	440	6	1.25	95.00	26.40
9	Centre	440	6	1.25	94.80	26.30

$$Y_2 = 26.03 - 5.86x_1 - 1.63x_2 + 3.36x_1^2 + 1.11x_2^2 - 1.39x_3^2 \quad (6)$$

The R^2 value of Eqs. (5) and (6) were 0.9995 and 0.9969, respectively, from which it can be concluded that both values are quite high, and this indicates that the predicted values for MB removal and PSAC yield are accurate and match the real values.

Statistical analysis and optimum conditions

ANOVA of the surface quadratic modelling results for MB removal and PSAC yield are provided in Tables 4 and 5, respectively. The significance of the variables are indicated by the F and P values, whereby the more significant effect of the corresponding variable is present if the F value is larger while the P value is smaller [34]. Values of P value < 0.05 showed that the model was significant. Table 4 shows that a corresponding Prob. $> F$ of less than 0.0001 for MB removal implies that this model is significant. Radiation power and IR were found to significantly affect MB removal, with radiation power having the greatest effect. The lack of fit

Table 4 ANOVA for the MB-removal response

Source	Sum of squares	Degree of freedom	Mean square	<i>F</i> value	<i>P</i> value Prob. > <i>F</i>
Model	5812.32	9	645.81	2257.23	< 0.0001
x_1	2957.37	1	2957.37	10,336.51	< 0.0001
x_2	0.0073	1	0.0073	0.025	0.8764
x_3	8.23	1	8.23	28.75	0.0003
x_1x_2	137.7	1	137.7	481.27	< 0.0001
x_1x_3	270.63	1	270.63	945.9	< 0.0001
x_2x_3	132.76	1	132.76	464.03	< 0.0001
x_1^2	817.87	1	817.87	2858.58	< 0.0001
x_2^2	30.78	1	30.78	107.57	< 0.0001
x_3^2	24.84	1	24.84	86.82	< 0.0001
Residual	2.86	10	0.29		
Lack of fit	1.77	5	0.35	1.62	0.3058
Pure error	1.09	5	0.22		
Cor total	5815.18	19			

Table 5 ANOVA for PSAC–yield response

Source	Sum of squares	Degree of freedom	Mean square	<i>F</i> value	<i>P</i> value Prob. > <i>F</i>
Model	428.24	9	47.58	352.4	< 0.0001
x_1	343.63	1	343.63	2544.98	< 0.0001
x_2	26.63	1	26.63	197.26	< 0.0001
x_3	0.16	1	0.16	1.18	0.3037
x_1x_2	0.54	1	0.54	4.01	0.0732
x_1x_3	0.036	1	0.036	0.27	0.6147
x_2x_3	0.00045	1	0.00045	0.333	0.9551
x_1^2	31.01	1	31.01	229.69	< 0.0001
x_2^2	3.38	1	3.38	25.01	0.0005
x_3^2	5.33	1	5.33	39.5	< 0.0001
Residual	1.35	10	0.14		
Lack of fit	0.98	5	0.2	2.67	0.1528
Pure error	0.37	5	0.074		
Cor total	429.6	19			

P value of 0.3058 showed that the lack of fit was ‘not significant’ and the regression model was effective for the MB adsorption onto PSAC. Similar results have been reported by other researchers [42, 43].

The value of Prob. $> F$ of less than 0.0001 listed in Table 5 indicates that the PSAC yield model is significant. Radiation power was found to have the greatest effect, followed by radiation time, while IR had an insignificant effect on PSAC yield. The P value of lack of fit around 0.1528 verifies the high efficiency and suitability of the model for fitting and justification of experimental data. The statistical results show that both models (Eqs. 5, 6) are adequate for predicting MB removal and PSAC yield within the range of variables studied.

Figure 1 shows the 3-D response surfaces that were constructed to show the effects of the two most important variables (radiation power and IR) on MB removal (Y_1). MB removal was observed to increase as the power was increased from 264 to 440 W and decrease as the radiation power was further increased to 616 W, which was due to small amounts of burnt-out carbon that blocked the pores of the sawdust surface after being decomposed at higher power. The MB removal capacity of the AC was observed to increase with increasing IR over the range of 0.5–2.00. This phenomenon is attributed to catalytic oxidation that increasingly widens the micropores to mesopores with increasing chemical IRs [44].

Figure 2 displays the 3-D response surface constructed to show the effect of the two most important variables (radiation power and radiation time) on PSAC yield (Y_2). PSAC yield was found to decrease with increasing radiation power and radiation time. The highest yield was obtained when both variables corresponded to minima over the range studied. The decreased yield at higher radiation power and radiation time is attributable to the impregnation of charcoal with KOH, which leads to the breakage of C–O–C and C–C bonds [45].

Optimum conditions were obtained at a radiation power of 418 W, a radiation time of 6.4 min, and an IR of 0.5. The predicted values for PSAC yield and MB removal were found to be 26.78 and 94.12%, respectively. The experimental values for PSAC yield and MB removal were 27 and 93.74%, which are in good agreement with the predicted values, with relatively small errors of 0.82 and 0.41%, respectively.

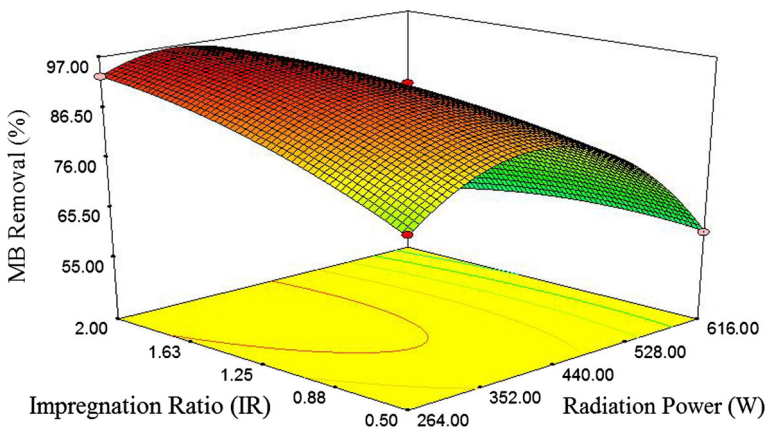


Fig. 1 Plot of 3-D surface for MB removal (effect of radiation power and IR, $t = 4$ min) by PSAC

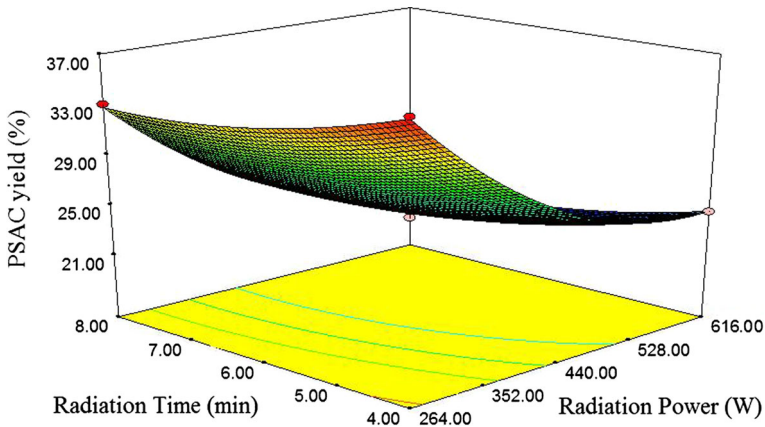


Fig. 2 Plot of 3-D surface of PSAC yield (effect of radiation time and radiation power, IR = 0.5)

Characterisation results

The BET surface area, total pore volume and average pore diameter of PSAC were found to be 914.15 m²/g, 0.52 cm³/g, and 3.19 nm, respectively. The average pore diameter of 3.19 nm shows that the activated carbon prepared in this manner is mesoporous, according to the IUPAC classification [46].

Figure 3 depicts the FTIR spectra of the PS and PSAC. The sawdust exhibits a variety of functional groups on its surface. The FTIR spectrum revealed the peaks at 3611–3951 cm⁻¹ ascribed to the presence of O–H stretching bands, which belong to hydroxyl groups. There was a broad peak at 2720 cm⁻¹ corresponding to C–H stretching vibrations of aliphatic carbon. The FTIR band at around 2335 cm⁻¹ is the C≡C stretching vibration of alkyne groups. The bands around 1689 and 1520 cm⁻¹ were assigned to carboxyl (C=O) and aromatic ring (C=C) stretching bands, respectively. The peak at 1269 cm⁻¹ was related to the C–O stretching of the phenolic group, while the bands below 1200 cm⁻¹ can be considered as a fingerprint region. On the other hand, the surface chemistry of PSAC can be seen to be different from that of PS, since many peaks were lost, which was related to breakdown of the cellulose and lignin structures during carbonisation and activation [47]. The surface chemistry of PSAC illustrates peaks at 3647 and 3734 cm⁻¹, which correspond to the presence of hydroxyl (O–H) groups, while the band at 1603 cm⁻¹ corresponds to stretching of the carboxyl (C=O) groups.

Table 6 shows the proximate analysis and elemental compositions of the PS and PSAC. The proximate analysis of PS showed the contents of moisture, ash, volatile matter and fixed carbon of 9.54, 2.44, 59.2 and 28.82% (of the dry mass), respectively. It was found that the percentage of volatile matter content was high, while the percentage of ash content was low for PS; this is a good feature for the production of mesoporous AC [47]. After the process of carbonisation and activation, volatile matter content was decreased to 15.13% while the carbon content increased to 78.31%, due to the discharge of volatile matter during chemical activation leading to the increase in carbon content. Elemental analysis results

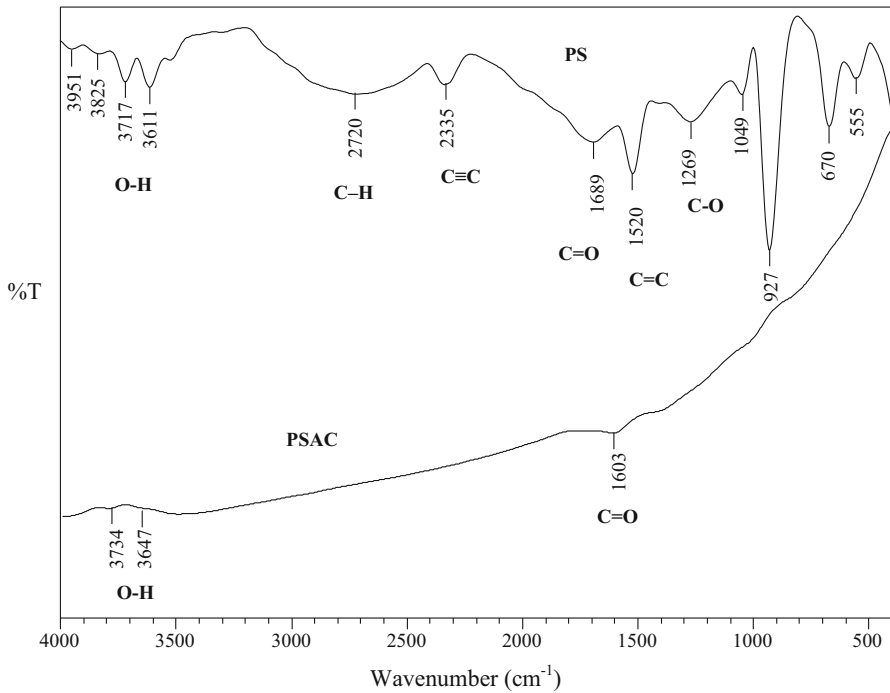


Fig. 3 FTIR spectra of the PS and PSAC

Table 6 Proximate analysis and elemental compositions

Sample	Proximate analysis (%)				Elemental analysis (%)			
	Moisture	Volatile	Fixed carbon	Ash	C	H	S	(N + O) ^a
PS	9.54	59.2	28.82	2.44	33.44	6.54	0.18	59.84
PSAC	4.39	15.13	78.31	2.17	79.34	2.48	0.09	18.09

^aEstimated by difference

showed that carbon compositions increased significantly from 33.44 to 79.34%, while other elements (H, S, N and O) were decreased after the activation process using microwave radiation. This is due to the breakdown of volatile components and the degradation of organic matter, aided by microwave radiation, to give high-purity carbon [9].

The SEM images of the PS and the PSAC prepared under optimum conditions are illustrated in Fig. 4a, b. The surface textures of the precursors were rough and uneven. On the other hand, pores of different sizes and different shapes are evident in the micrograph of PSAC. The chemical activation process had succeeded in producing pores on the carbon surface as well as producing AC with large surface area and a porous structure.

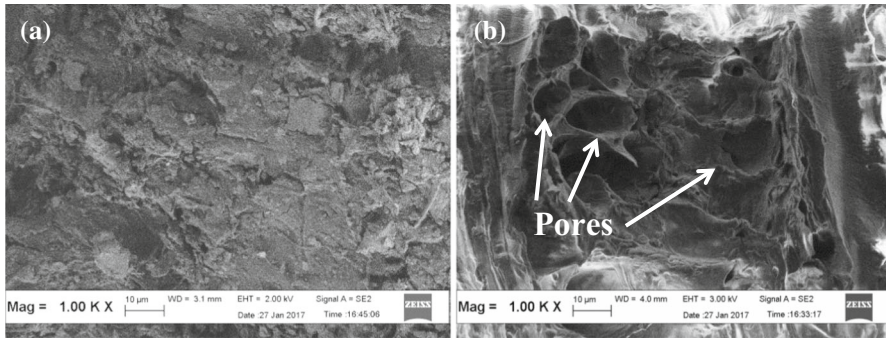


Fig. 4 Scanning electron micrographs of **a** PS and **b** PSAC at $\times 1000$ magnification

Effect of initial pH value

Due to the importance of monitoring the pH effect in adsorption, the initial pH effect on MB dye removal by PSAC was studied in the range 2–12, as illustrated in Fig. 5. In batch mode, 0.2 g of PSAC was added to 200 mL of a solution of MB dye at a concentration of 100 mg/L at 30 °C. The pH of the solution was adjusted in the range 2–12 by using 0.1 M HCl or 0.1 M NaOH solutions. From the figure, MB dye removal can be seen to increase with the increase in the pH value of the MB dye solution.

This reveals that pH affects the ionic state of the dye molecules and/or the functional groups or charges of the activated carbon [48]. Characterisation of the PSAC revealed the presence of hydroxyl ($-\text{OH}$) and carboxyl ($-\text{COOH}$) groups. Figure 6a–c shows the possible mechanism of interaction of PSAC with MB dye molecules in different pH conditions. In the neutral state, the reaction mechanism

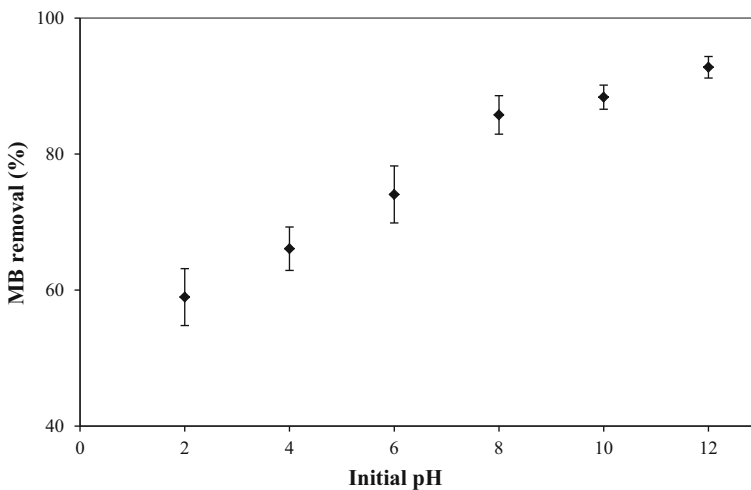


Fig. 5 The pH effect on the adsorption of MB onto PSAC

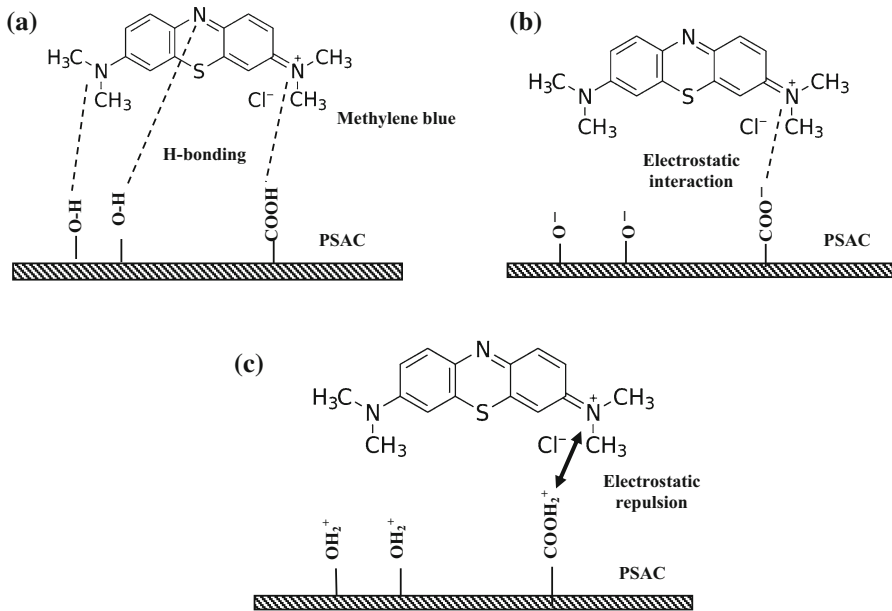


Fig. 6 Possible PSAC–MB dye interaction under different pH conditions: **a** neutral, **b** basic, and **c** acidic

occurs via hydrogen bonding between the $-OH$ and $-COOH$ groups on the PSAC surface with the nitrogen atoms of the MB dye. In the basic state, the hydroxyl and carboxyl groups on the surface of PSAC are deprotonated and the number of negatively charged groups increases, causing an increase in the electrostatic interaction between the negatively charged PSAC and the positively charged MB molecule. In contrast, under acidic conditions the hydroxyl and carboxyl functional groups of the PSAC are protonated and become more positively charged. In this state, the adsorption efficiency is consequently reduced because of the strong electrostatic repulsion between the positively charged MB molecules and the positively charged PSAC. Thus, it can be concluded that the adsorption of MB dye by the PSAC is efficient in basic conditions. Similar trends have been observed in the use of white pine sawdust-based activated carbon for the adsorption of MB dye [30]. The maximum adsorption percentage of MB removal was 92.8% at pH 12.

Adsorption isotherms

Table 7 summarises parameters obtained when six isotherm models are applied to the adsorption of MB dye on PSAC at 30 °C. With respect to R^2 value (in descending order): Redlich–Peterson > Sips > Langmuir > Freundlich > Temkin > Dubinin–Radushkevich. With respect to χ^2 (in descending order): Redlich–Peterson > Langmuir > Freundlich > Temkin > Dubinin–Radushkevich > Sips. Based on those results (i.e., Lowest χ^2 and highest R^2), it was revealed that Redlich–Peterson was the best fitting model with an $R^2 = 0.9998$ and $\chi^2 = 0.25$, followed by the Langmuir model ($R^2 = 0.9946$ and $\chi^2 = 0.4$).

Table 7 Parameters of isotherm models for the adsorption of MB onto PSAC at 30 °C

Model	Parameters	Values at 30 °C
Langmuir	Q_m (mg/g)	357.14
	K_L (L/mg)	0.019
	R^2	0.9946
	χ^2	0.40
Freundlich	K_F (mg/g) (L/mg) ^{1/n}	9.92
	n_F (l/mg)	1.369
	R^2	0.9897
	χ^2	6.30
Temkin	A	0.289
	B (L/g)	86.94
	R^2	0.9511
	χ^2	106.16
Dubinin–Radushkevich	E (kJ/mol)	0.354
	q_D (mg/g)	138.75
	R^2	0.7491
	χ^2	112.75
Redlich–Peterson	K_R (L/g)	6.197
	α_R (l/mg) ^g	0.0054
	g	0.996
	R^2	0.9998
	χ^2	0.25
Sips	q_s (mg/g)	313.72
	K_s (dm ³ /mmol)	0.0174
	n_s	0.902
	R^2	0.9995
	χ^2	121.31

The Redlich–Peterson model is a hybrid adsorption mechanism that combines three types of parameters in its empirical isotherm and consists of elements of the Langmuir and Freundlich models, which recognise monolayer and multilayer adsorption. When the exponent values of the Redlich–Peterson model, g , is equivalent to zero, the equation follows Henry's Law, while when $g \approx 1$ it follows the Langmuir equation [49]. As can be seen in Table 7, $g = 0.996$, which approaches unity; hence, corresponding to the original Langmuir equation. By adhering to the Langmuir isotherm model, the adsorption process occurs in a monolayer. The R_L value from the Langmuir model for all concentrations in this study (25–300 mg/L) were in the range of 0–1, indicating that the adsorption of MB on the PSAC occurs favourably [49]. The profiles for all adsorption models are shown in Fig. 7.

Table 8 shows a comparison of the maximum monolayer adsorption capacities of MB dye calculated by the Langmuir model for a variety of adsorbents. It can be seen

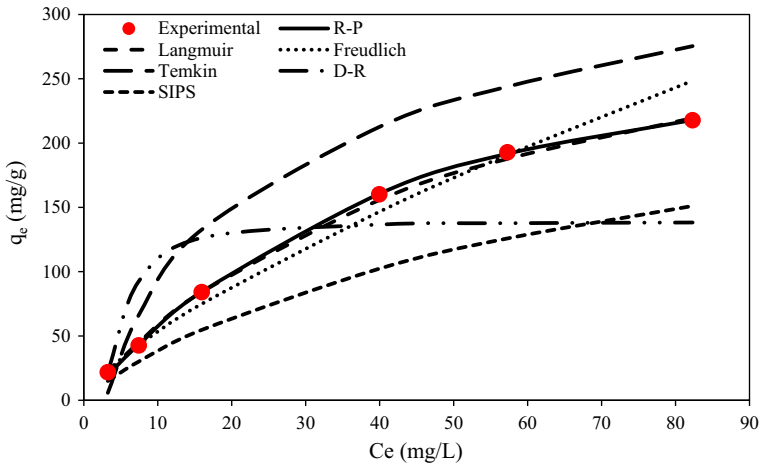


Fig. 7 Isotherm plots for MB adsorption onto PSAC (conditions: temperature 30 °C, pH 7)

Table 8 Maximum monolayer adsorptions of MB dye onto different adsorbents

Precursor	Activation method	Activating reagent	S _{BET} (m ² /g)	Total pore volume (cm ³ /g)	Pore structure	Q _m (mg/g)	References
Pentace species sawdust	Microwave heating	KOH	914.15	0.520	Mesoporous	357.14	This study
Pineapple peel	Microwave heating	KOH	1006.00	0.590	Mesoporous	462.10	[50]
Rattan	Conventional heating	NaOH	1135.00	0.600	Mesoporous	359.00	[51]
Karanj fruit hulls	Conventional heating	KOH	828.30	0.360	Microporous	239.40	[52]
Macadamia endocarp	Microwave heating	ZnCl ₂	600.00	0.300	Microporous	194.70	[49]
Oil palm ash	Conventional heating	NaOH	615.41	0.575	Mesoporous	143.47	[53]
Chitosan flake	Conventional heating	NaOH	318.40	0.255	Mesoporous	121.45	[54]

that MB adsorption capacities of the adsorbent used in this work (357.14 mg/g) is relatively high, especially for systems that use microwave heating activation. The higher adsorption efficiency could be derived from the high porosity and higher surface area (914.15 m²/g) of the PSAC, which provide more sites for adsorption of MB compared to other ACs (< 900 m²/g). The high adsorption efficiency is beneficial and indicates the potential for the AC to be used as a dye adsorbent.

Adsorption kinetics

The experimental data obtained for the adsorption of MB using six different initial concentrations of MB dye were fitted to PFO, PSO, and Elovich models at 30 °C. The results of these fittings are shown in Fig. 8, which shows that rapid adsorption occurred over the first hour at each of the six concentrations, with equilibrium reached after 6 h, indicating that the adsorbent surface and adsorbate molecules interact favourably.

Table 9 lists the kinetic parameters obtained from the kinetic models. As presented, at all studied concentrations (25–300 mg/L) the q_e values of the PSO

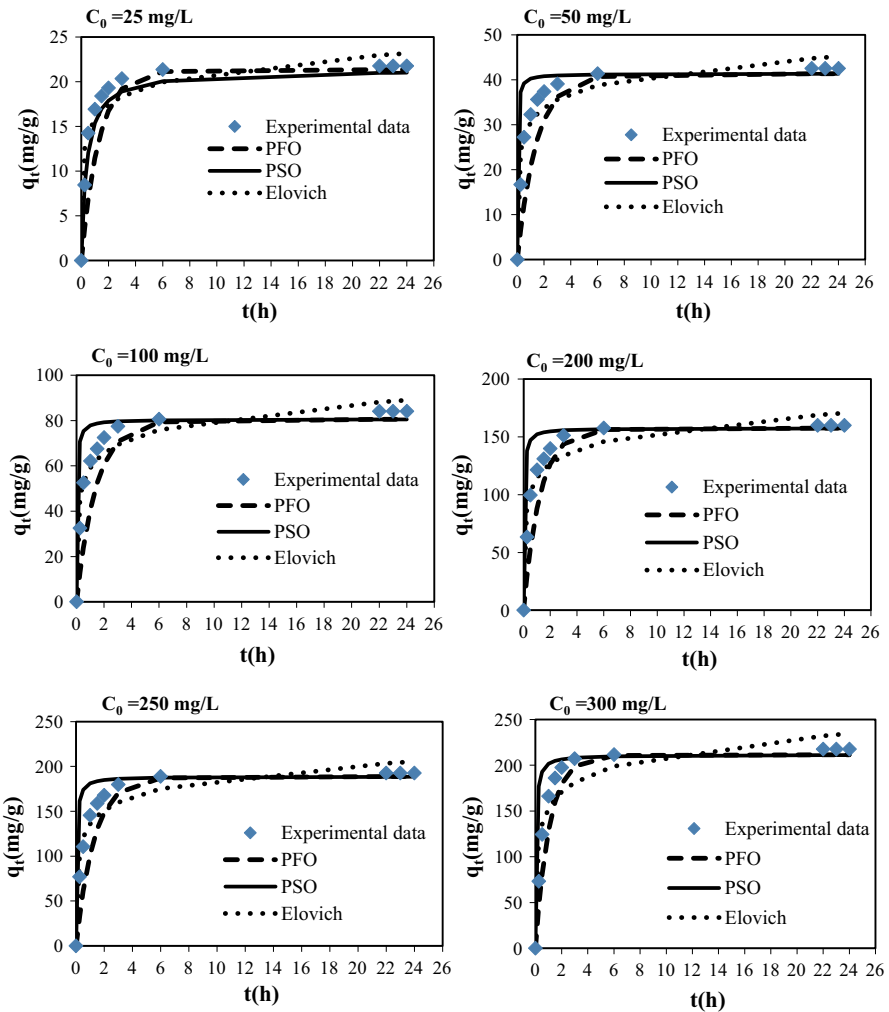


Fig. 8 PFO, PSO and Elovich-kinetic models for the adsorption of MB onto PSAC at different initial concentrations, C_0 (conditions: temperature 30 °C, pH 7)

Table 9 Kinetic parameters for the adsorption of MB-PSAC at various initial concentrations

Parameters	C_0 (mg/L)					
	25	50	100	200	250	300
$q_{e,exp}$ (mg/g)	21.76	42.58	84.06	160.04	192.71	217.69
<i>PFO model</i>						
k_1 (1/h)	0.77	0.70	0.70	0.82	0.78	0.94
q_e (mg/g)	12.08	23.28	49.52	99.59	120.02	149.26
R^2	0.9511	0.9360	0.9692	0.9834	0.9796	0.9751
Δq (%)	44.48	45.33	41.09	37.77	37.72	31.43
<i>PSO model</i>						
k_2 (g/mg h)	0.12	0.87	0.35	0.18	0.13	0.10
q_e (mg/g)	22.83	43.67	84.03	166.67	200.00	227.27
R^2	0.9985	1.0000	0.9999	0.9999	0.9999	0.9999
Δq (%)	4.93	2.57	0.03	4.14	3.78	4.40
<i>Elovich model</i>						
α (mg/g h)	2125.76	3439.66	5051.14	11,664.08	10,940.87	9826.07
B (g/mg)	0.43	0.22	0.11	0.06	0.05	0.04
R^2	0.7835	0.8116	0.8395	0.8113	0.8220	0.7594
q_e (mg/g)	23.17	45.19	88.98	170.51	205.42	234.50
Δq (%)	6.50	6.15	5.86	6.54	6.60	7.72
<i>Intraparticle diffusion model</i>						
k_{r1} (mg/g h ^{1/2})	19.55	37.54	72.65	138.31	156.04	170.31
C_1	0.30	0.47	0.86	1.30	2.49	2.70
R^2	0.9839	0.9890	0.9902	0.9938	0.9998	0.9828
k_{r2} (mg/g h ^{1/2})	4.61	9.10	21.10	40.77	46.90	55.27
C_2	12.56	23.90	41.55	81.16	100.04	115.01
R^2	0.9708	0.9370	0.9860	0.9965	0.9873	0.9350
k_{r3} (mg/g h ^{1/2})	0.17	0.51	1.47	1.54	1.63	2.60
C_3	20.94	40.12	77.00	155.08	184.88	205.22
R^2	0.9948	0.9948	0.9948	0.9948	0.9948	0.9948

model are more closely correlated with the experimental values ($q_{e,exp}$), indicating that this model best describes the adsorption behaviour of MB on PSAC. Furthermore, the average value of R^2 for the PSO model (0.9997) is higher than those of PFO and Elovich models, at 0.9657 and 0.8046, respectively. These results show that adsorption of MB onto PSAC is best described by the PSO model, which exhibited an R^2 value close to unity, the lowest values of Δq (0.03–4.93%), and close agreement between the q_e values determined by the model and experiment. This suggests chemisorption is the rate-limiting step in the MB–PSAC system.

The plots of the intraparticle diffusion model are shown in Fig. 9. If intraparticle diffusion plays a role in the adsorption process, the plot of q_t versus $t^{1/2}$ will be a

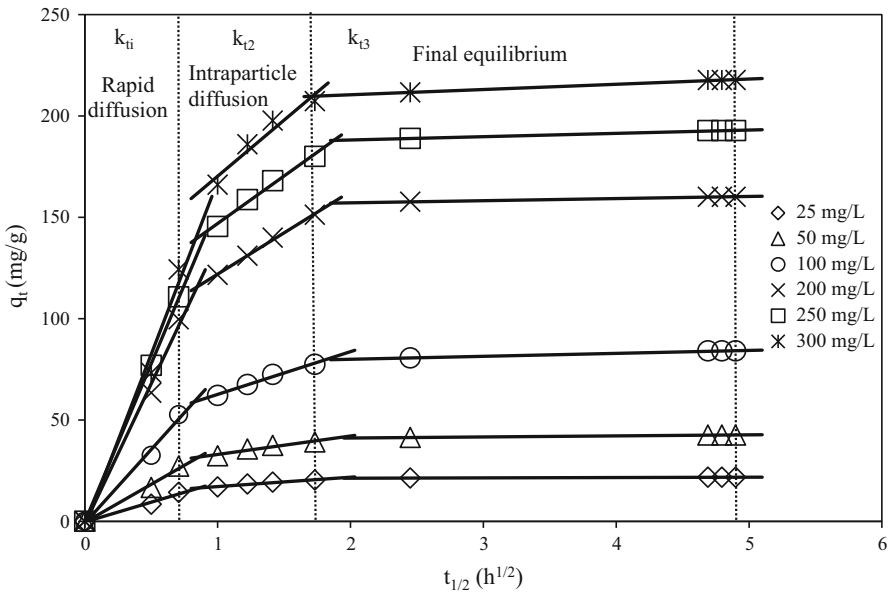


Fig. 9 Intraparticle diffusion model of MB adsorption onto PSAC

straight line, and if this line crosses the origin, then intraparticle diffusion is the rate-limiting step [53]. However, as shown in Fig. 9, the diffusion mechanism resulted in three straight lines for all studied concentrations, and all the three lines do not pass through the origin. Thus, in this case, intraparticle diffusion is not the only step in determining rates. From the figure, the diffusion mechanism can be divided into three phases: rapid diffusion, intraparticle diffusion and final equilibrium. From the point of origin to the third point (first 0.5 h), instantaneous diffusion, so-called rapid diffusion, occurs and is due to strong electrostatic attraction between the MB solution and the outer surface of the adsorbent. In the second stage (1–3 h), the phenomenon of penetration of molecules into the inner layers of adsorbent occurs gradually; this phenomenon is called intraparticle diffusion. The gradual smooth transition from phase 1 to phase 2 implies the diffusion of MB dye molecules from the macropores to the mesopores [55]. The final phase (after 3 h) is called the final equilibrium phase, where the diffusion begins to occur slowly with reduced concentration of MB.

Table 9 shows the parameters of the intraparticle diffusion model, where it can be observed that for each different concentration the value of k_{ti} decreased when the time increased. This proves that external mass transfer is inversely proportional to time [34]. Meanwhile, the value of C increased when the concentration and time increased, which means that the boundary layer thickness increases with concentration and time. The high value of R^2 shows the suitability of this model to explain the experimental data.

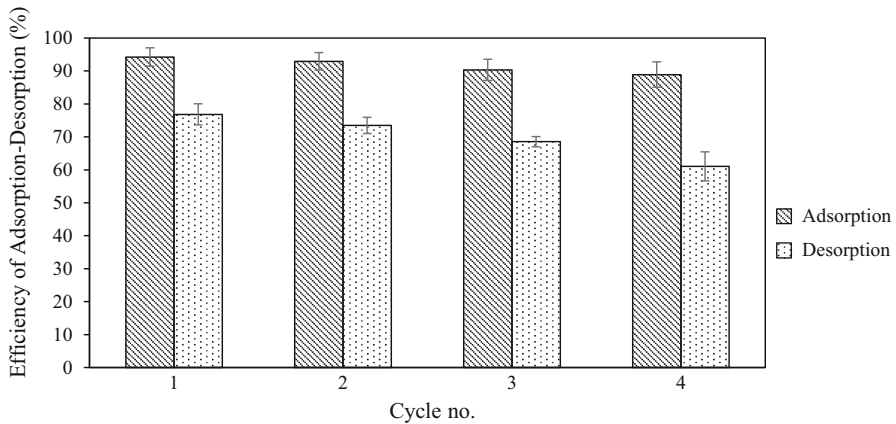


Fig. 10 Regeneration performance of PSAC

Regeneration tests

Tests of effectiveness after four cycles of regeneration of the carbon were 94.24, 92.93, 90.34 and 88.89% for adsorption and 76.82, 73.46, 68.55 and 61.07% for desorption, respectively. The results in Fig. 10 clearly show that the PSAC can be reused continually without a substantial loss in its MB adsorption capacity. The MB adsorption efficiency for PSAC was reduced from 94.24 to 88.89% after four cycles of adsorption–desorption process, which implies that the PSAC can be used successfully at least four times for removal of MB from aqueous solution.

Conclusions

The MB dye removal and percentage yield of PSAC were found to agree satisfactorily with the model predictions. Optimum conditions for the preparation of PSAC were: a radiation power of 418 W, radiation time of 6.4 min, and IR of 0.5, which resulted in a 27% yield of PSAC and a 93.74% efficiency of MB dye removal. The adsorption behaviour of MB dye on PSAC is best described by pseudo-second-order kinetic, intraparticle diffusion and Redlich–Peterson adsorption models. The results of this study confirm that PS is a promising and feasible precursor for the manufacture of activated carbon with significant dye-removal capacity.

Acknowledgements The authors express their gratitude to Universiti Sains Malaysia under the Iconic grant scheme (Grant No. 1001/CKT/870023) for research associated with the Solid Waste Management Cluster and Bridging grant (304.PJKIMIA.6316100).

References

1. A. Regti, M.R. Laamari, S.-E. Stiriba, M. El Haddad, *Microchem. J.* **130**, 129 (2017)
2. S. Dawood, T.K. Sen, *J. Chem. Proc. Eng.* **1**, 1 (2014)
3. F. Aeenjan, V. Javanbakht, *Res. Chem. Intermed.* **44**, 1459 (2017)
4. H. Saygılı, F. Güzel, *Ecotoxicol. Environ. Saf.* **131**, 22 (2016)
5. O. Pezoti, A.L. Cazetta, I.P.A.F. Souza, K.C. Bedin, A.C. Martins, T.L. Silva, V.C. Almeida, *J. Ind. Eng. Chem.* **20**, 4401 (2014)
6. H. Kamandari, H. Hashemipour Rafsanjani, H. Najjarzadeh, Z. Eksiri, *Res. Chem. Intermed.* **41**, 71 (2015)
7. N.T. Abdel-Ghani, G.A. El-Chaghaby, M.H. Elgammal, E.S.A. Rawash, Xinxing Tan Cailiao/New Carbon Mater. **31**, 492 (2016)
8. M.J. Ahmed, S.K. Theydan, *J. Anal. Appl. Pyrolysis* **99**, 101 (2013)
9. M.A. Ahmad, N.A. Ahmad Puad, O.S. Bello, *Water Resour. Ind.* **6**, 18 (2014)
10. V.O. Njoku, K.Y. Foo, M. Asif, B.H. Hameed, *Chem. Eng. J.* **250**, 198 (2014)
11. R. Subramaniam, S. Kumar Ponnusamy, *Water Resour. Ind.* **11**, 64 (2015)
12. P.S. Thue, M.A. Adebayo, E.C. Lima, J.M. Sieliechi, F.M. Machado, G.L. Dotto, J.C.P. Vaghetti, S.L.P. Dias, *J. Mol. Liq.* **223**, 1067 (2016)
13. R. Hoseinzadeh Hesas, W.M.A. Wan Daud, J.N.N. Sahu, A. Arami-Niya, *J. Anal. Appl. Pyrolysis* **100**, 1 (2013)
14. N. Adilla Rashidi, S. Yusup, *Chem. Eng. J.* **314**, 277 (2016)
15. G.S. Dos Reis, M. Wilhelm, T.C.D.A. Silva, K. Rezwan, C.H. Sampaio, E.C. Lima, S.M.A.G.U. De Souza, *Appl. Therm. Eng.* **93**, 590 (2016)
16. A.F. Abbas, M.J. Ahmed, *J. Water Process Eng.* **9**, 201 (2016)
17. J. Mohammed, N.S. Nasri, M.A.A. Zaini, U.D. Hamza, H.M. Zain, F.N. Ani, *Desalin. Water Treat.* **57**, 7881 (2015)
18. R. Hoseinzadeh Hesas, A. Arami-Niya, W.M.A. Wan Daud, J.N. Sahu, *Chem. Eng. Res. Des.* **91**, 2447 (2013)
19. J. Georgin, G.L. Dotto, M.A. Mazutti, E.L. Foletto, *J. Environ. Chem. Eng.* **4**, 266 (2016)
20. G. Li, J. Li, W. Tan, H. Jin, H. Yang, J. Peng, C.J. Barrow, M. Yang, H. Wang, W. Yang, *Int. Biodeterior. Biodegrad.* **113**, 386 (2016)
21. A. Kundu, B. Sen Gupta, M.A. Hashim, G. Redzwan, *J. Clean. Prod.* **105**, 420 (2015)
22. H.P.S.A. Khalil, N.A.S. Aprilia, A.H. Bhat, M. Jawaid, M.T. Paridah, D. Rudi, *Renew. Sustain. Energy Rev.* **22**, 667 (2013)
23. L. Muniandy, F. Adam, A.R. Mohamed, E.P. Ng, *Microporous Mesoporous Mater.* **197**, 316 (2014)
24. K.Y. Foo, B.H. Hameed, *Bioresour. Technol.* **111**, 425 (2012)
25. P.S. Thue, G.S. dos Reis, E.C. Lima, J.M. Sieliechi, G.L. Dotto, A.G.N. Wamba, S.L.P. Dias, F.A. Pavan, *Res. Chem. Intermed.* **43**, 1063 (2017)
26. M.A.F. Mazlan, Y. Uemura, S. Yusup, F. Elhassan, A. Uddin, A. Hiwada, M. Demiya, *Proc. Eng.* **148**, 530 (2016)
27. M. Ghaedi, H. Mazaheri, S. Khodadoust, S. Hajati, M.K. Purkait, *Spectrochim. Acta Part A Mol. Biomol. Spectrosc.* **135**, 479 (2015)
28. A. Jain, S. Jayaraman, M. Ulaganathan, R. Balasubramanian, V. Aravindan, M.P. Srinivasan, S. Madhavi, *Electrochim. Acta* **228**, 131 (2017)
29. F. Kazemi, H. Younesi, A.A. Ghoreyshi, N. Bahramifar, A. Heidari, *Process Saf. Environ. Prot.* **100**, 22 (2016)
30. J.J. Salazar-Rabago, R. Leyva-Ramos, J. Rivera-Utrilla, R. Ocampo-Perez, F.J. Cerino-Cordova, *Sustain. Environ. Res.* **27**, 32 (2016)
31. Y.P. Huang, C.H. Hou, H.C. Hsi, J.W. Wu, *J. Taiwan Inst. Chem. Eng.* **50**, 266 (2015)
32. R. Boopathy, S. Karthikeyan, A.B. Mandal, G. Sekaran, *Environ. Sci. Pollut. Res.* **20**, 533 (2013)
33. T. Bohli, A. Ouederni, *Environ. Sci. Pollut. Res.* **23**, 15852 (2016)
34. B. Zhang, X. Han, P. Gu, S. Fang, J. Bai, *J. Mol. Liq.* **238**, 316 (2017)
35. H. Kalavathy, B. Karthik, L.R. Miranda, *Colloids Surf. B Biointerfaces* **78**, 291 (2010)
36. A.B. Albadarin, M.N. Collins, M. Naushad, S. Shirazian, G. Walker, C. Mangwandi, *Chem. Eng. J.* **307**, 264 (2017)
37. M.V. Subbaiah, D.S. Kim, *Ecotoxicol. Environ. Saf.* **128**, 109 (2016)
38. H. Sharififard, F. Pepe, P. Aprea, B. de Gennaro, *Res. Chem. Intermed.* **43**, 6553 (2017)

39. J.R. Garcia, U. Sedran, M.A.A. Zaini, Z.A. Zakaria, *Environ. Sci. Pollut. Res.* **25**, 5076 (2017)
40. A.M. Aljeboree, A.N. Alshirifi, A.F. Alkaim, *Arab. J. Chem.* **10**, S3381 (2017)
41. W. Tanthapanichakoon, P. Ariyadejwanich, P. Japthong, K. Nakagawa, S.R. Mukai, H. Tamon, *Water Res.* **39**, 1347 (2005)
42. M.A. Ahmad, R. Alrozi, *Chem. Eng. J.* **165**, 883 (2010)
43. I.A.W. Tan, A.L. Ahmad, B.H. Hameed, *Chem. Eng. J.* **137**, 462 (2008)
44. B.H. Hameed, I.A.W. Tan, A.L. Ahmad, *J. Hazard. Mater.* **158**, 324 (2008)
45. M.A. Ahmad, R. Alrozi, *Chem. Eng. J.* **168**, 280 (2011)
46. R.L. Burwell, *Pure Appl. Chem.* **46**, 71 (1976)
47. K.K. Beltrame, A.L. Cazetta, P.S.C. de Souza, L. Spessato, T.L. Silva, V.C. Almeida, *Ecotoxicol. Environ. Saf.* **147**, 64 (2018)
48. T. Maneerung, J. Liew, Y. Dai, S. Kawi, C. Chong, C.H. Wang, *Bioresour. Technol.* **200**, 350 (2016)
49. O. Pezoti Junior, A.L. Cazetta, R.C. Gomes, E.O. Barizao, I.P.A.F. Souza, A.C. Martins, T. Asefa, V.C. Almeida, *J. Anal. Appl. Pyrolysis* **105**, 166 (2014)
50. K.Y. Foo, B.H. Hameed, *Microporous Mesoporous Mater.* **148**, 191 (2012)
51. M.A. Islam, M.J. Ahmed, W.A. Khanday, M. Asif, B.H. Hameed, *Ecotoxicol. Environ. Saf.* **138**, 279 (2017)
52. M.A. Islam, S. Sabar, A. Benhouria, W.A. Khanday, M. Asif, B.H. Hameed, *J. Taiwan Inst. Chem. Eng.* **74**, 96 (2017)
53. W.A. Khanday, F. Marrakchi, M. Asif, B.H. Hameed, *J. Taiwan Inst. Chem. Eng.* **70**, 32 (2017)
54. F. Marrakchi, M.J. Ahmed, W.A. Khanday, M. Asif, B.H. Hameed, *Int. J. Biol. Macromol.* **98**, 233 (2017)
55. X. Duan, C. Srinivasakannan, X. Wang, F. Wang, X. Liu, *J. Taiwan Inst. Chem. Eng.* **70**, 374 (2016)